

海洋大循環モデリングにおける 「渦」パラメタリゼーションの様々な側面

東京大学気候システム研究センター

羽角博康

Contents:

- 海洋大循環の実態と成因
- 海洋大循環モデリングの必要性
- 海洋大循環モデル開発の焦点
- 個々の「渦」パラメタリゼーションについて
(水平混合、鉛直混合、鉛直対流、境界層...)

海洋大循環の(多分に推定を含む)実態と成因

「地球流体」としての海洋の特徴

- 流れに対して「器の形」の制約が大きい
- 比較的「濃い」塩水であり、塩分の変化幅は密度変化に対して重要
- 外力項が海洋内部でほとんど無視できる
- …

海洋の流れ場の直接的な観測: 不可能ではないが簡単でもない
船舶、漂流ブイ、フロート、ADCP、流速計、…

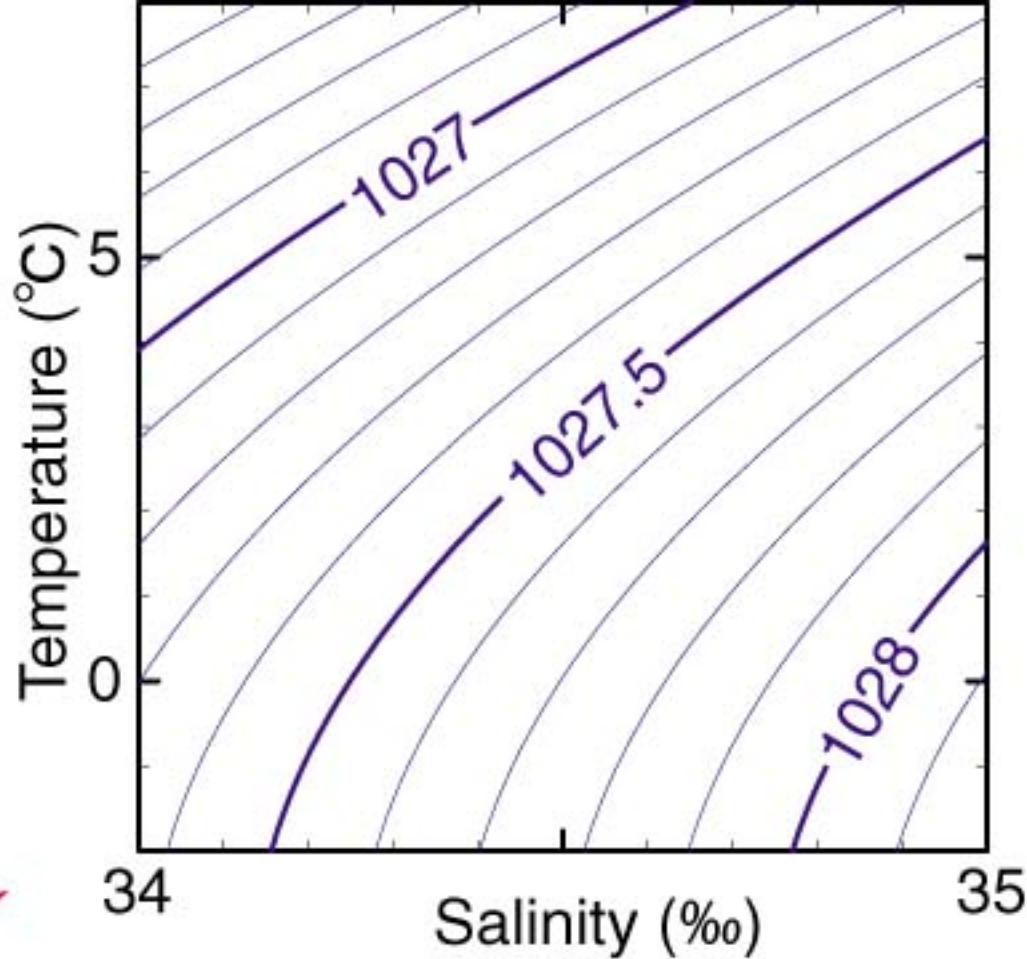
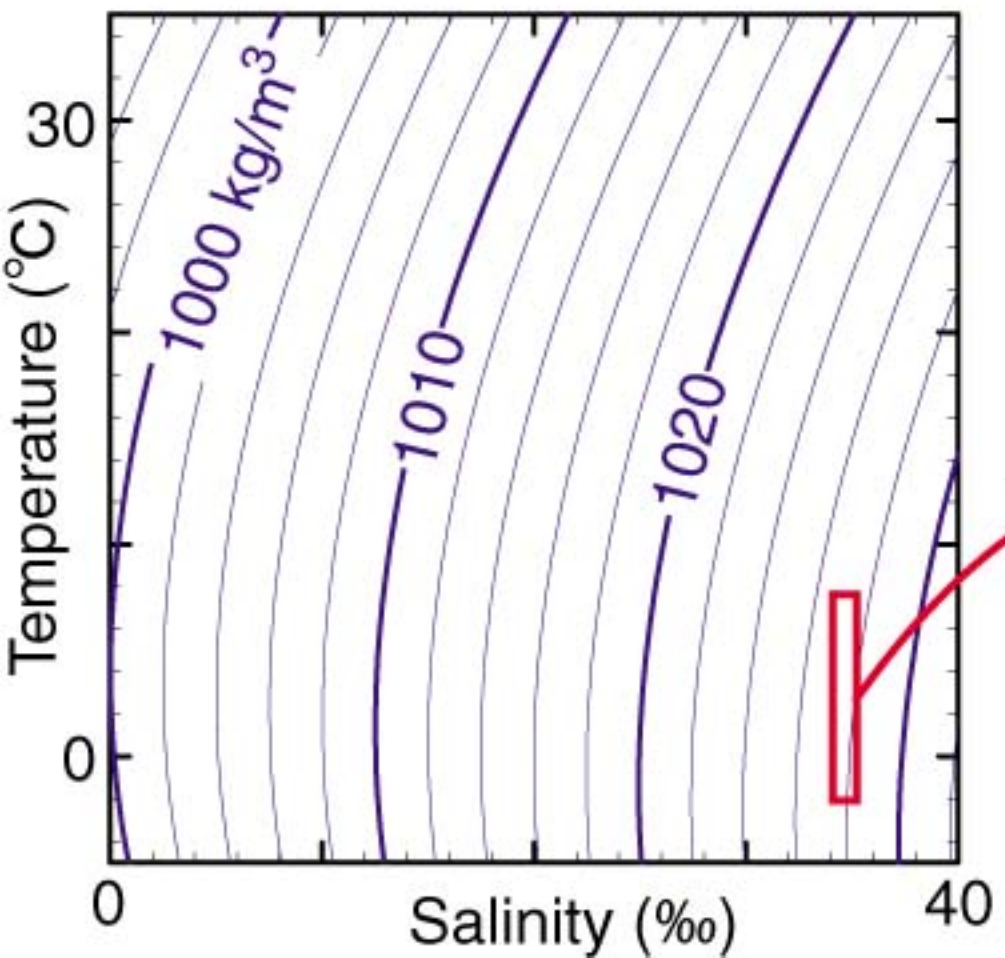
海洋の流れ場の間接的な推定

地衡流計算、トレーサー分布、モデリング、…

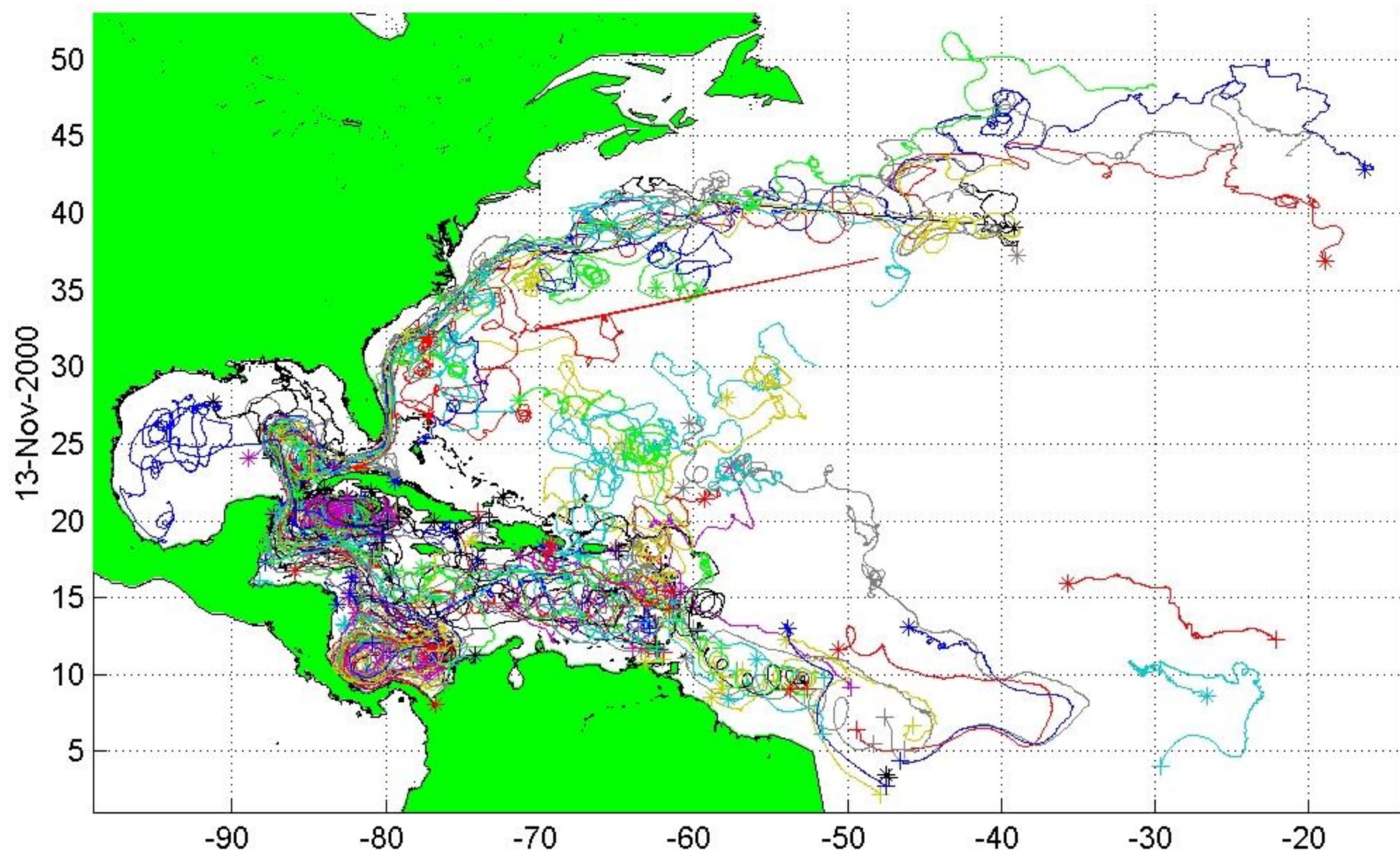
海洋大循環の概観

上層: 風成循環

深層: 熱塩循環



IAS YOTO ALL Drifter Tracks



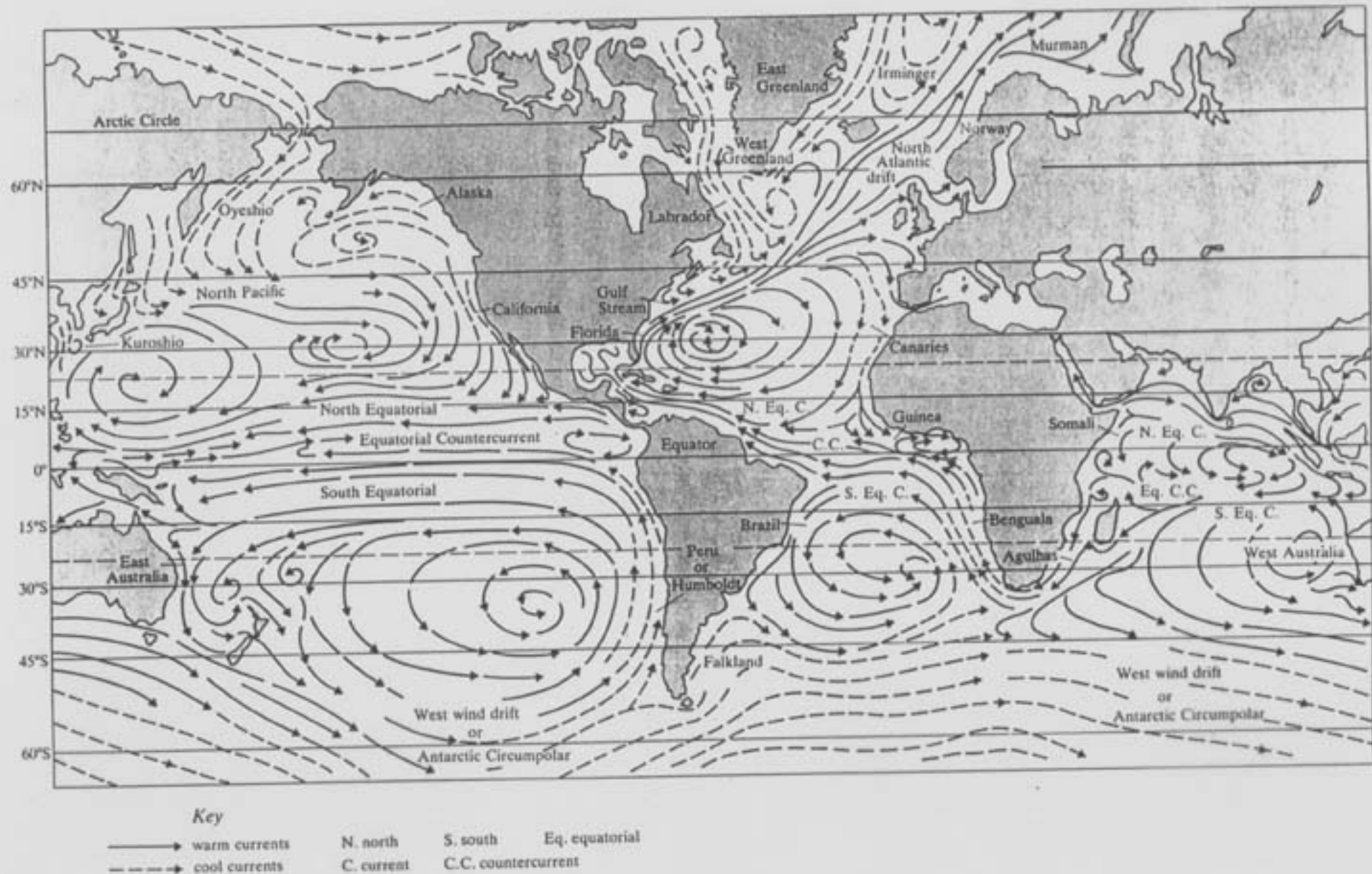
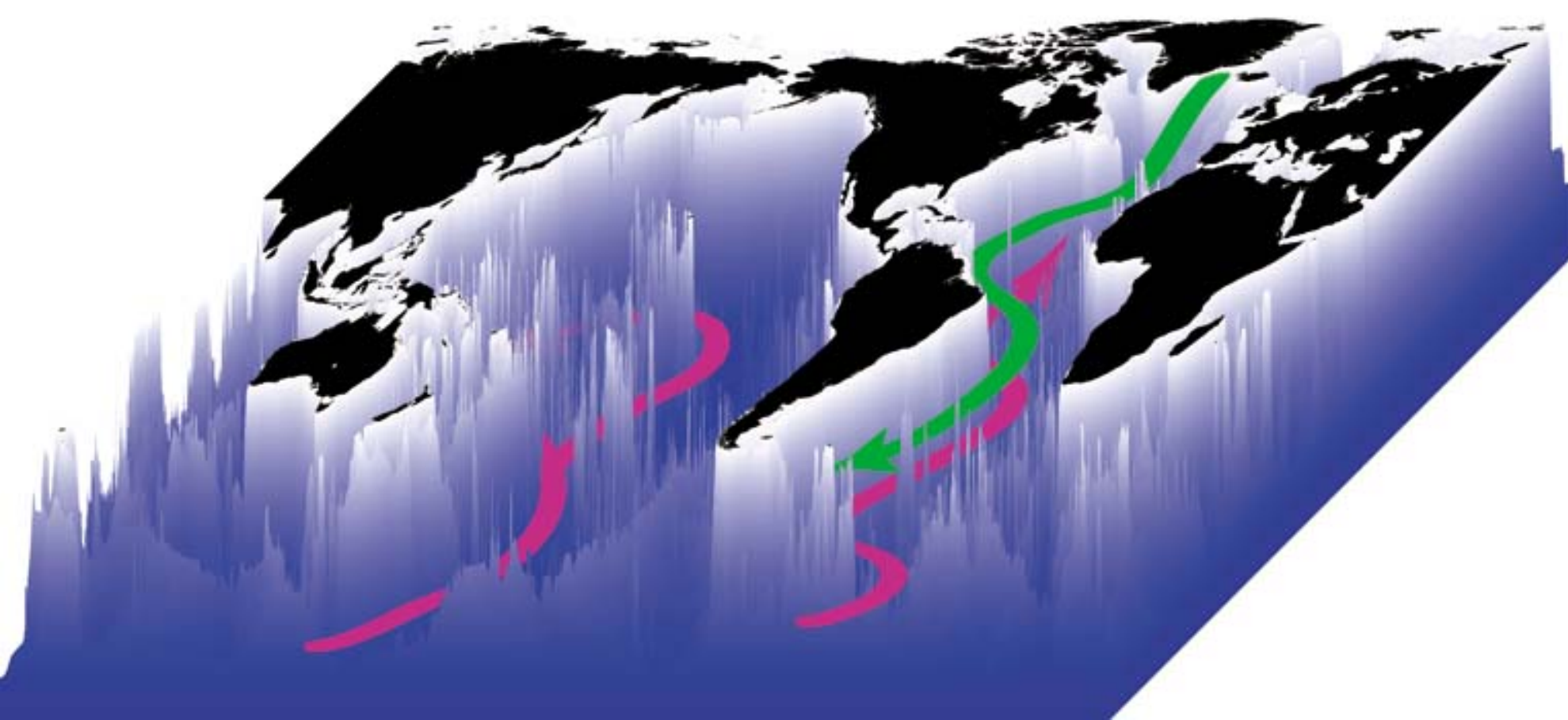


Figure 1-3. A map of the major currents of the world ocean (after Tomazin 1985). The horizontal dashed lines are the Tropic of Cancer at 23.5°N and the Tropic of Capricorn at 23.5°S. The Arctic Circle and the Antarctic Circle are at 66.5°N and 66.5°S respectively.



海洋物理学的な問題意識とは

水塊という考え方

観測された水塊分布をもたらす流れ場とそのメカニズム

- Active tracer から

- Passive tracer から

海洋大循環モデリングの必要性

海洋大循環モデリングとは何か

なぜ大循環モデリングでなければならないのか

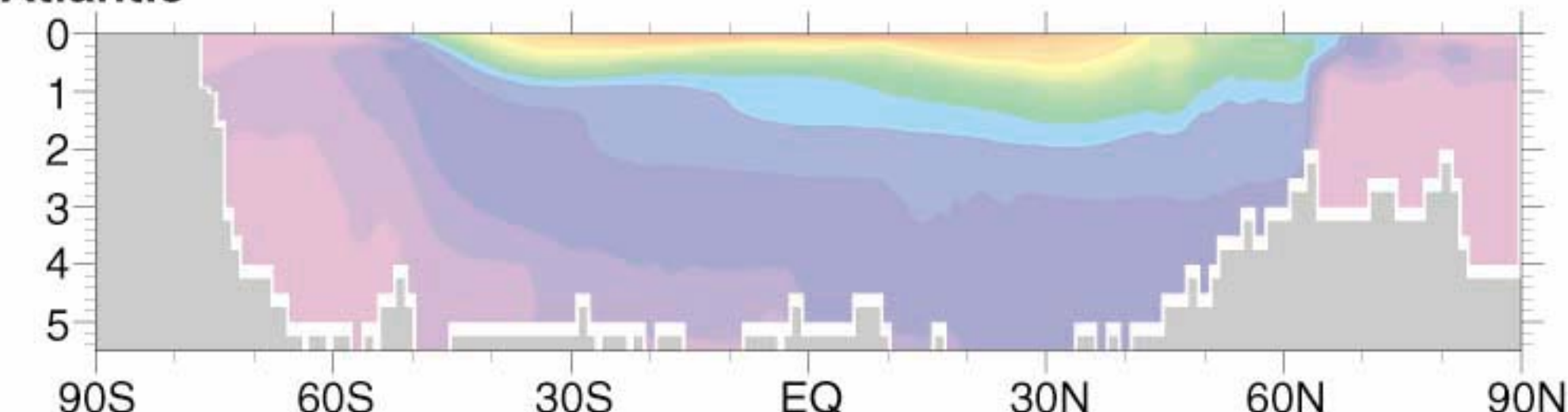
- 非線型・非断熱過程の重要性

- 現実の水塊分布の説明

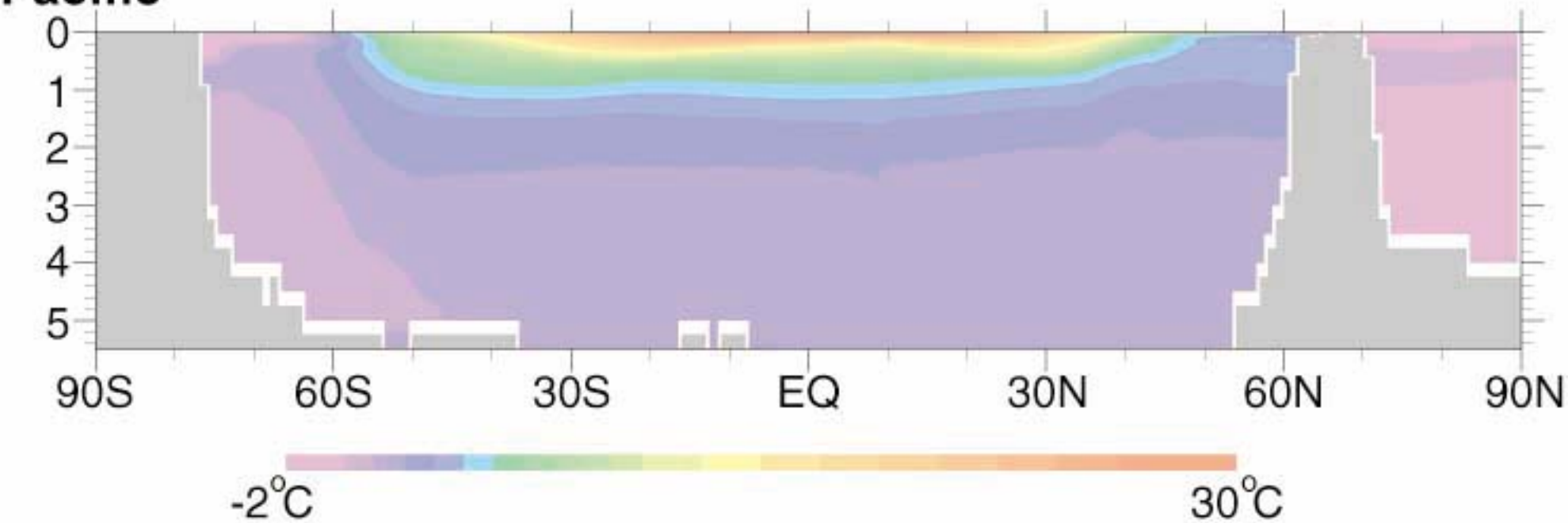
- 変動予測

Zonal-mean Temperature

Atlantic

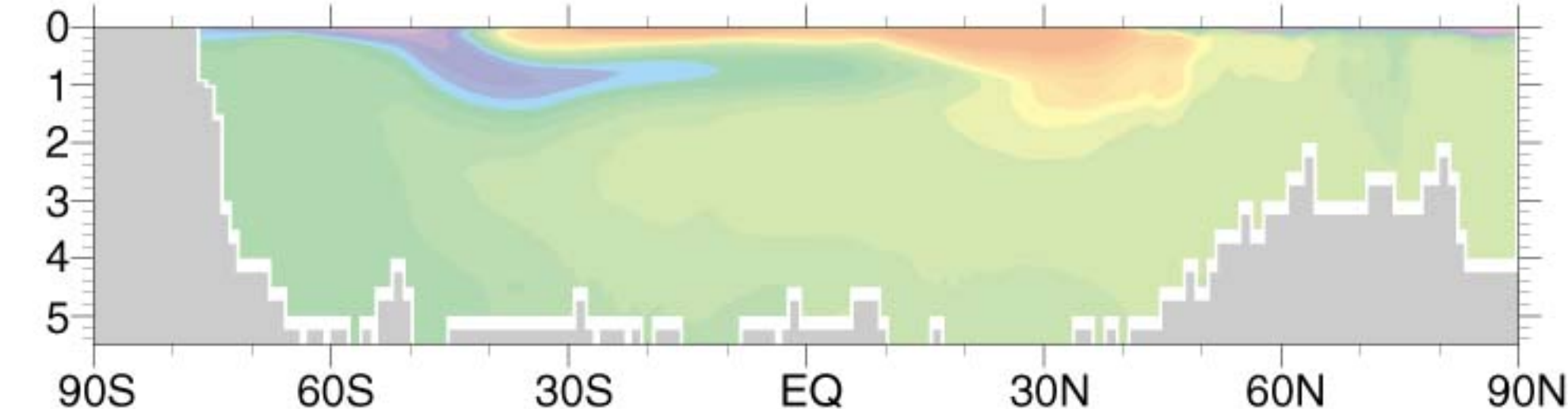


Pacific

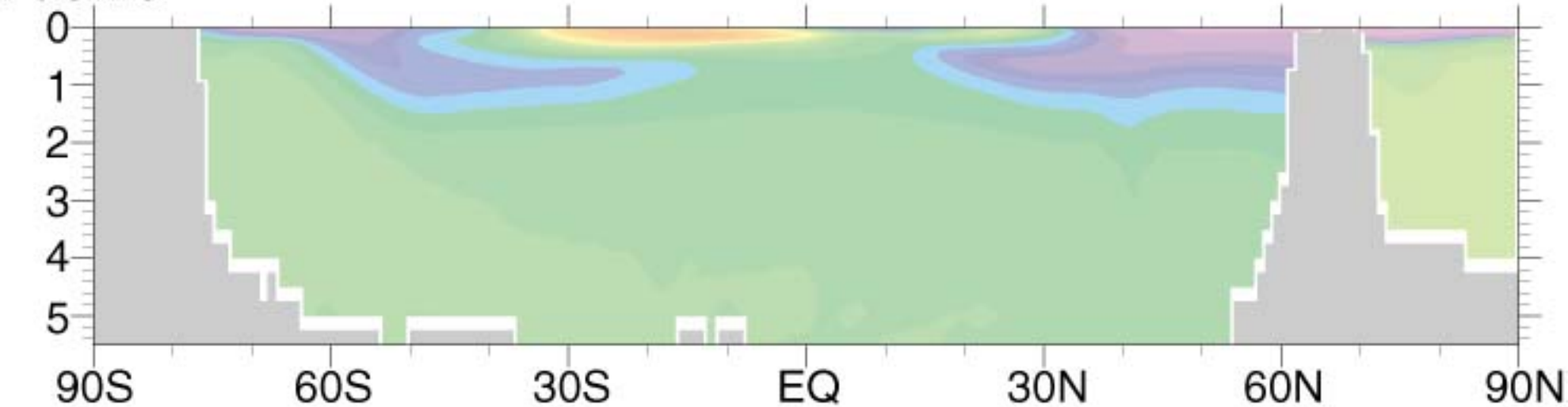


Zonal-mean Salinity

Atlantic



Pacific

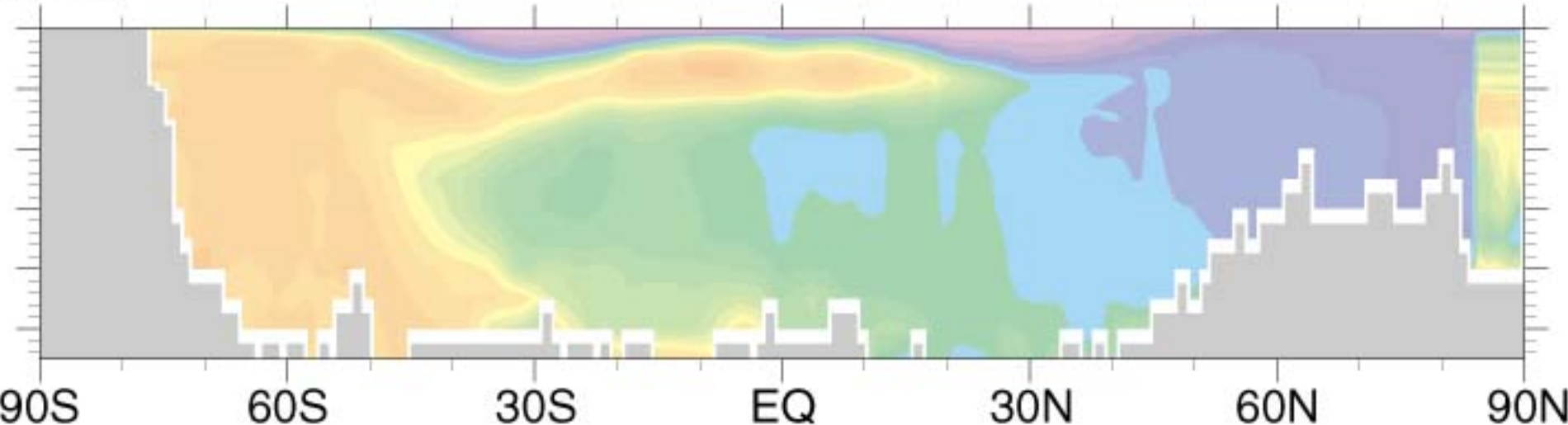


33psu

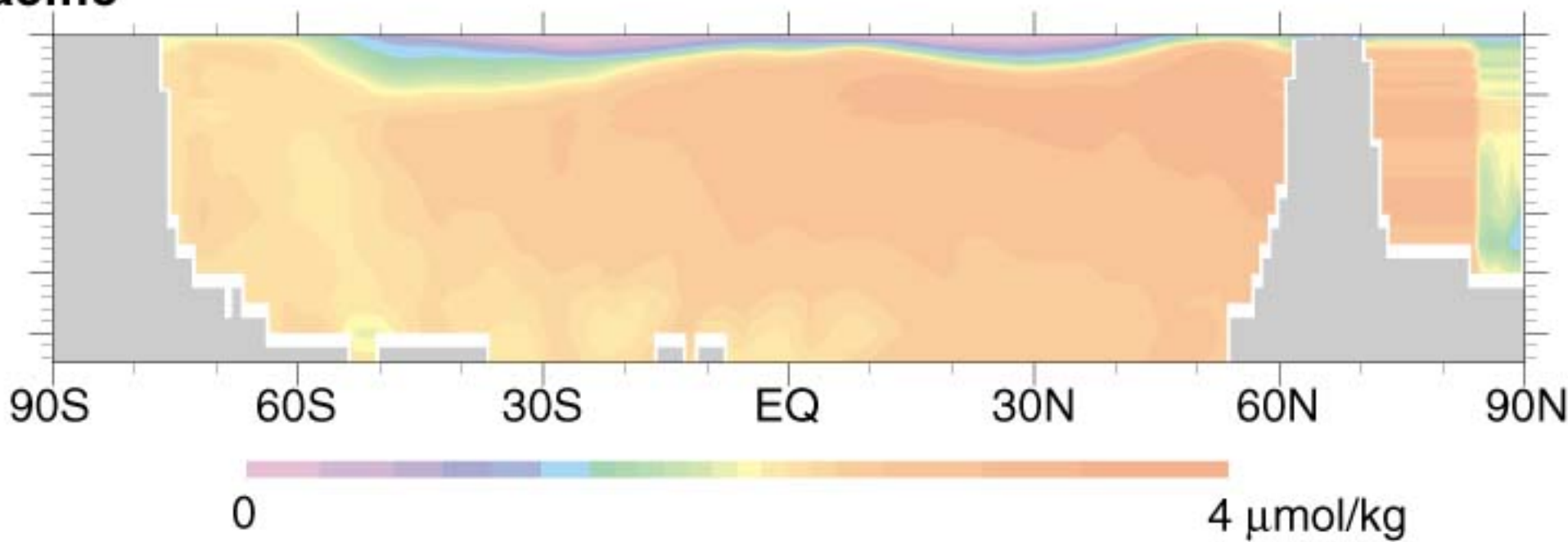
37psu

Zonal-mean Phosphate

Atlantic



Pacific

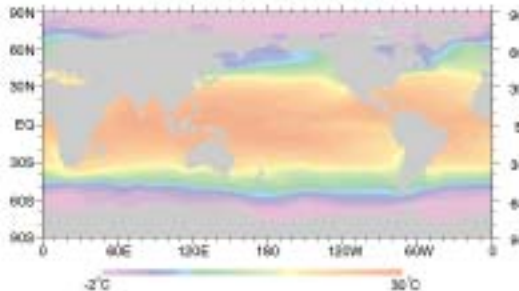


海面水温

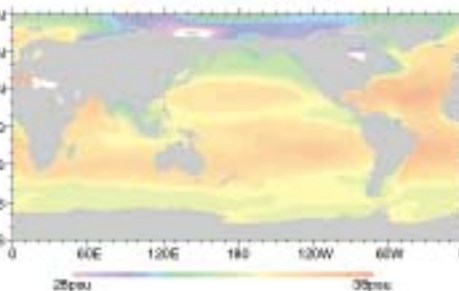
海面塩分

海面風応力

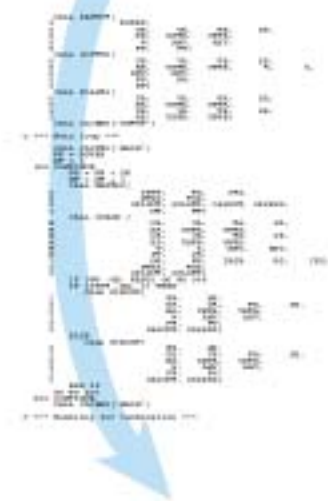
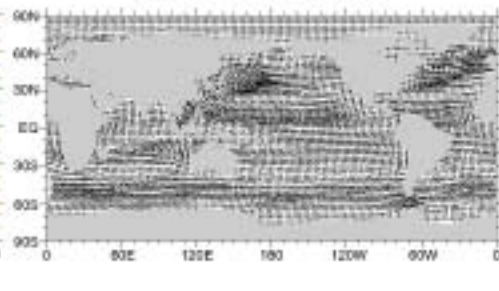
Sea Surface Temperature



Sea Surface Salinity

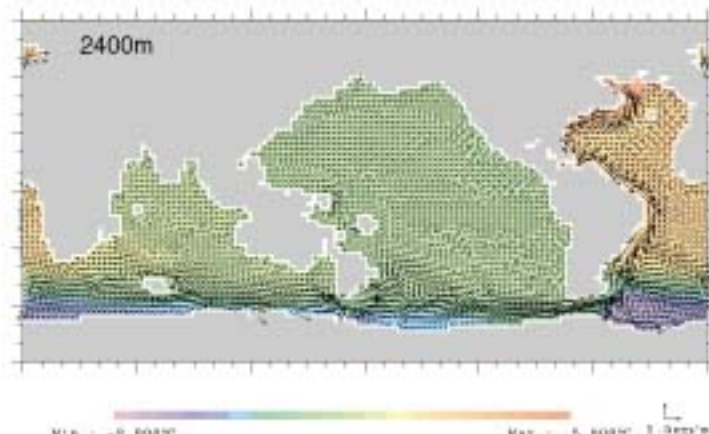
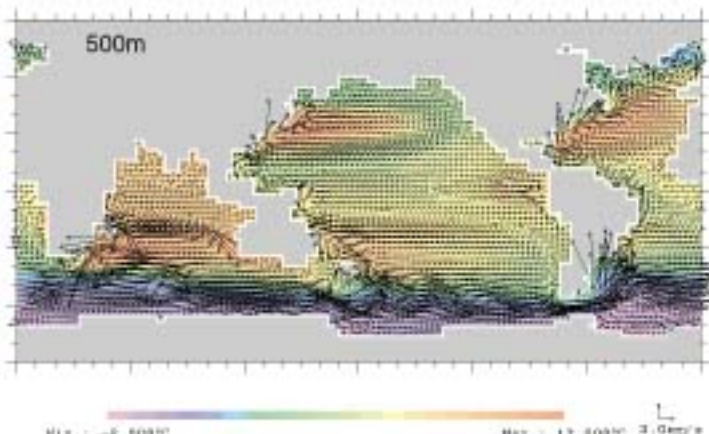


Sea Surface Wind Stress



海洋大循環モデル

海洋内部の温度・塩分・流れ



観測データとの比較・検証（相補的）

海洋の循環等の構造を決める
物理的プロセスの理解

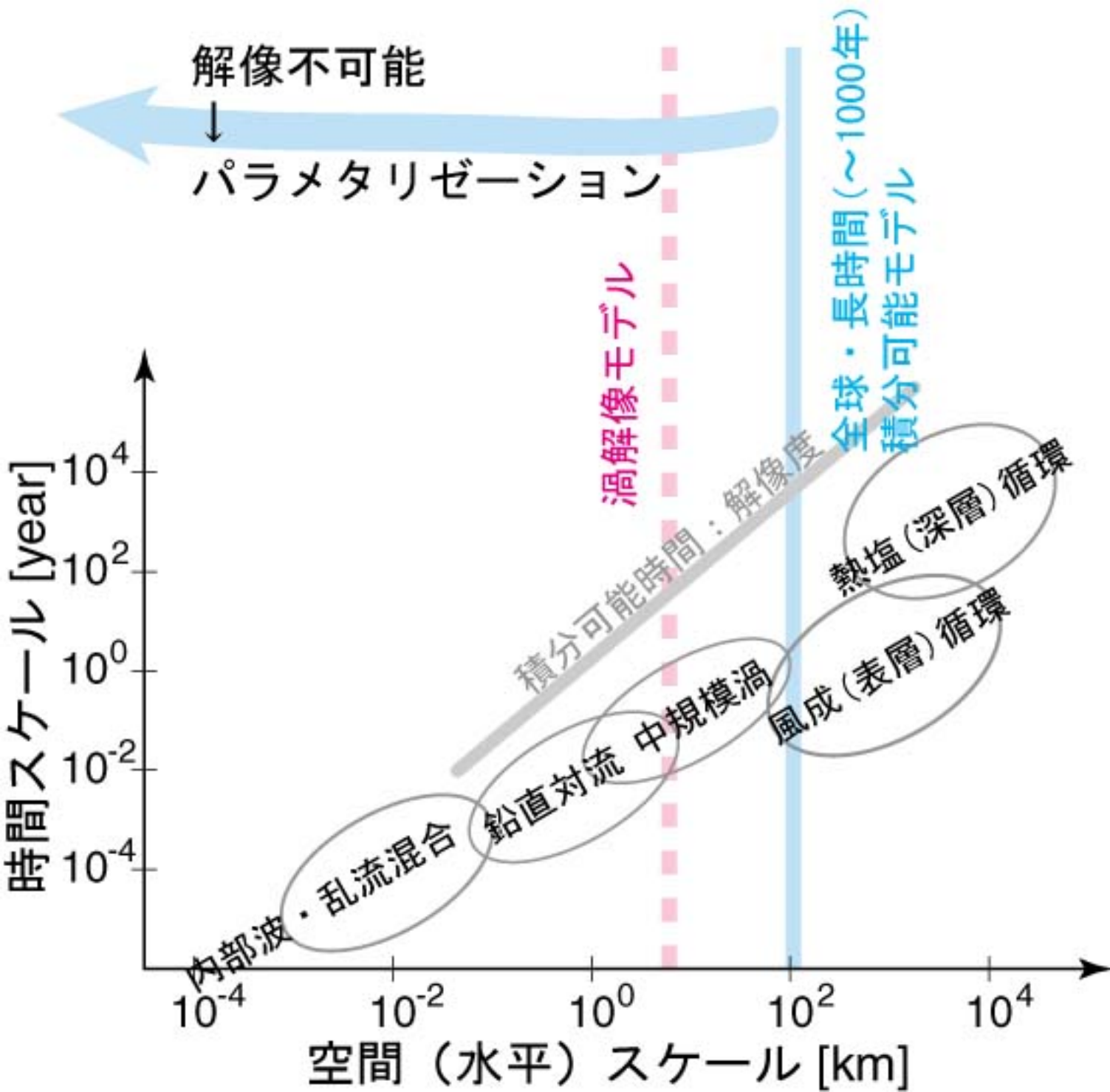
海洋大循環モデル開発の焦点

解像度とパラメタリゼーション

海洋大循環モデリングにおける「渦」混合過程の重要性

具体的には...

- 水平渦混合: 中規模渦
- 乱流渦の地形による「整流」
- 鉛直渦混合: 内部重力波、二重拡散対流
- 鉛直対流
- 海面境界層: 風波、Langmuir 循環
- 海底境界層: 中規模渦、エントレインメント、海底エクマン層



水平渦混合: 中規模渦による攪拌

海洋における中規模渦の実態

- 観測から
- 高解像度モデリングの結果から

海洋大循環における中規模渦の役割

海洋大循環モデルにおける中規模渦のパラメタリゼーション

- 等密度面混合
- Gent-McWilliams パラメタリゼーション



CoastWatch

AVHRR Temperature

Filename: E9716211.HD?

DMGMAP Simage

NOAA 12 Orbit: 31535

SATIRBT JD 162 11:27:00MT

Pixel Size: 4.17 km

Lat Range: 29.84N to 45.82N

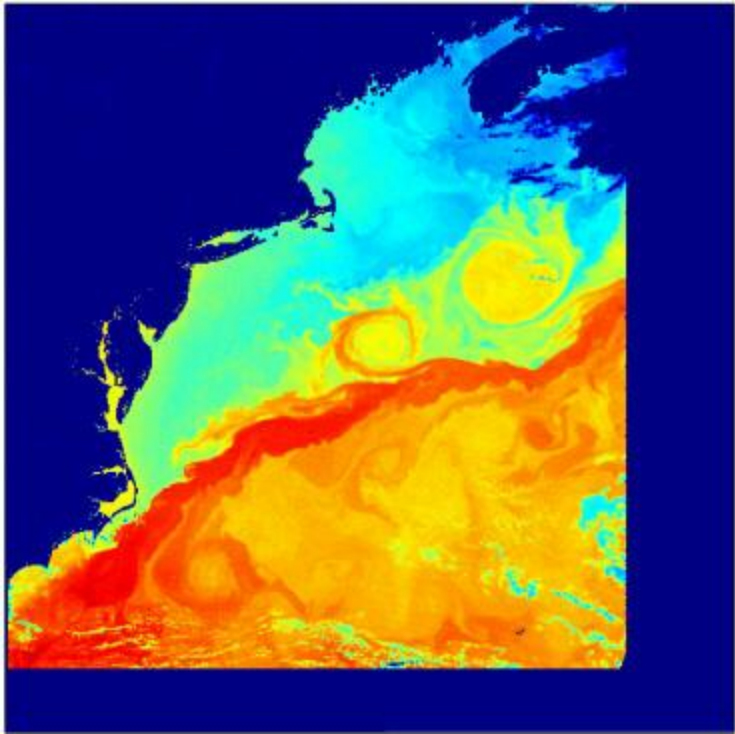
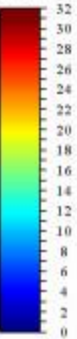
Lon Range: 79.88W to 58.81W

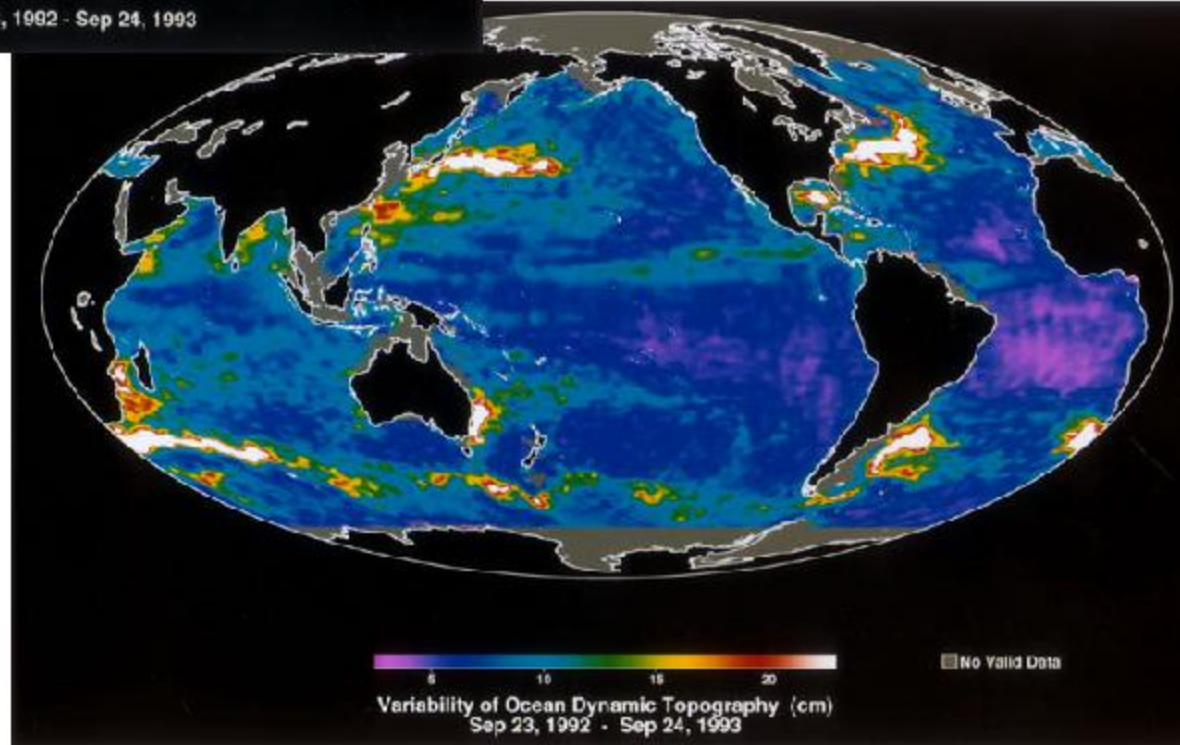
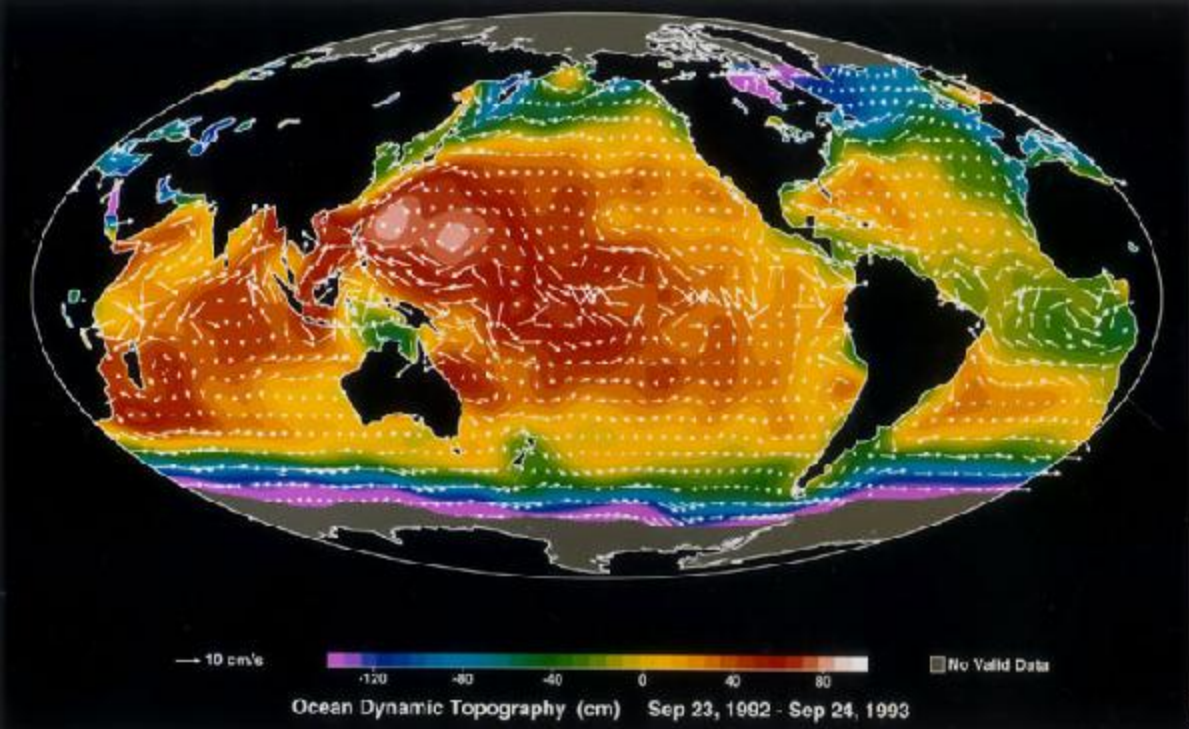
Horiz. Offset: -1994 2

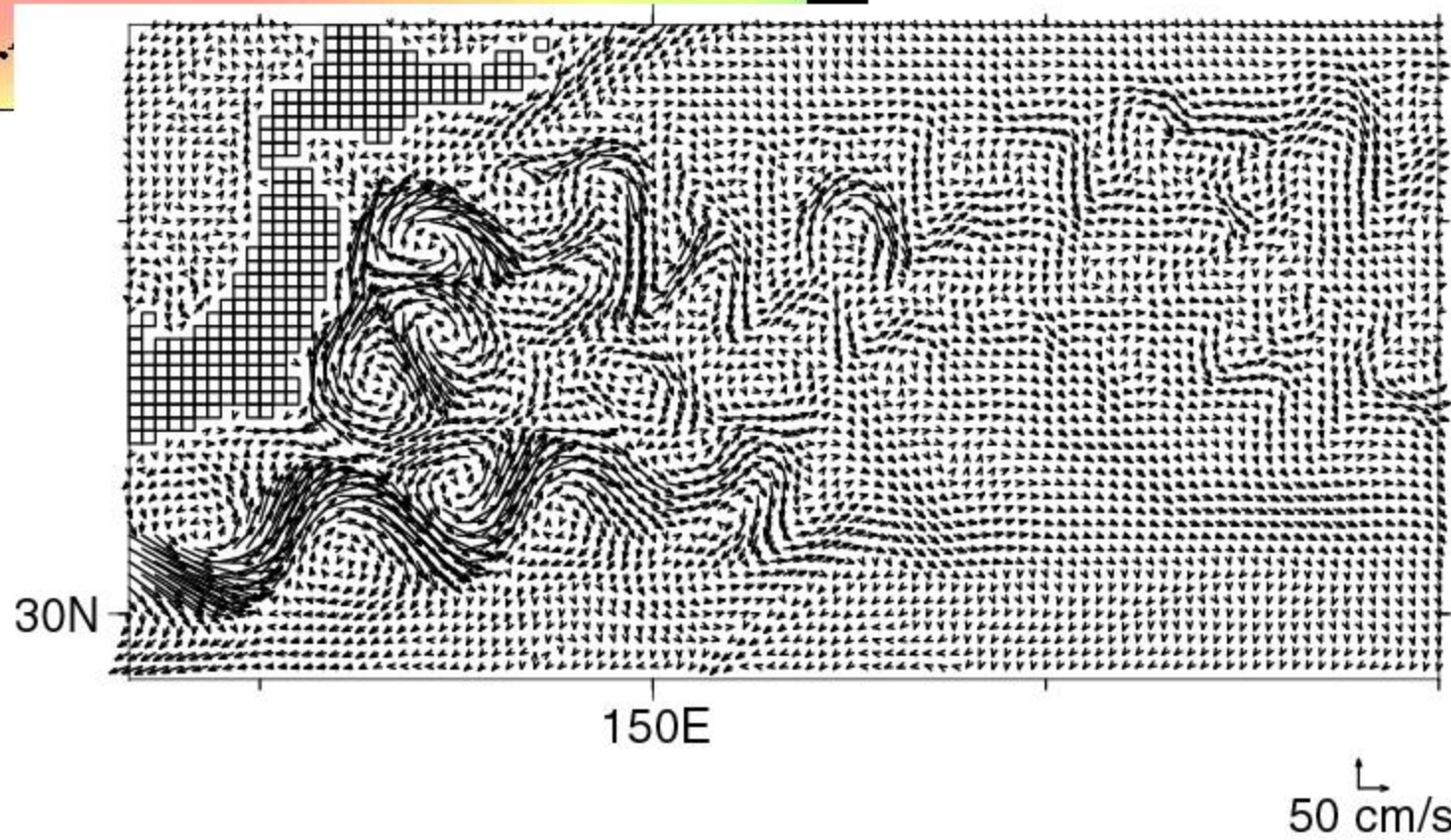
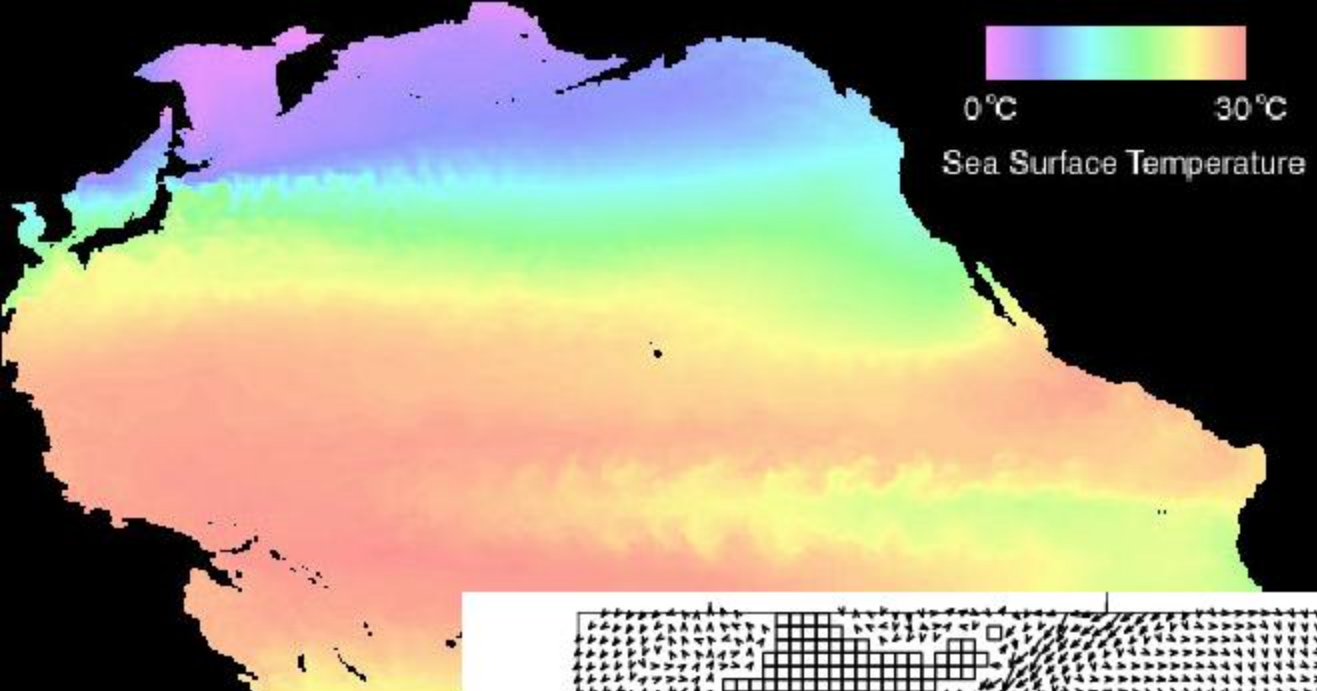
Vert. Offset: 4681 6

EST - Split Window

Surface Temperature
(Degrees Centigrade)







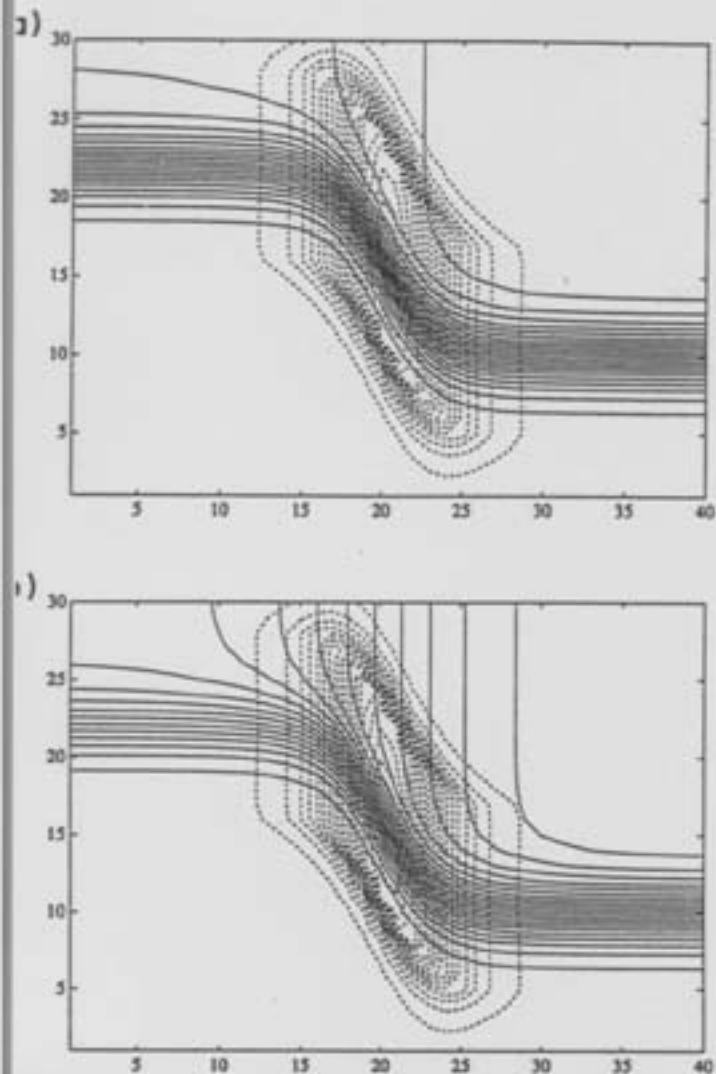


FIG. 3. Initial states of (a) temperature and (b) salt [contour interval one-quarter that of (a)]. Both panels also show the streamfunction ϕ_s/ρ_s for the parameterized eddy-induced transport velocity.

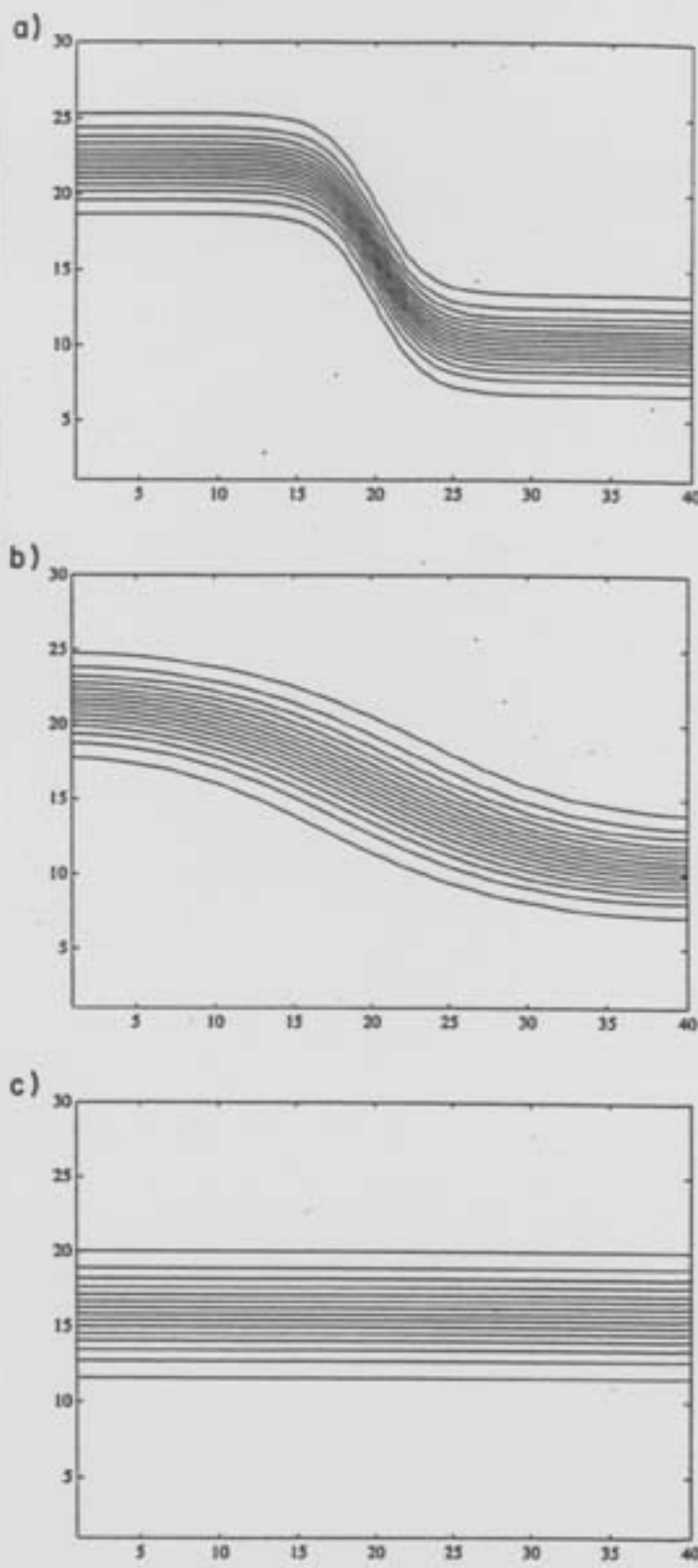


FIG. 5. Density distribution at various times of the integration.
(a) Initial, (b) $20\Delta x^2/\kappa$, and (c) $1000\Delta x^2/\kappa$.

Neptune 効果: 亂流渦の地形による整流

基本発想

渦に地形が作用することによって生じる応力が平均流を生み出す

一例として…

北極海の表・中層循環

海洋大循環モデルにおけるパラメタリゼーションの方法

定量化できるのか？

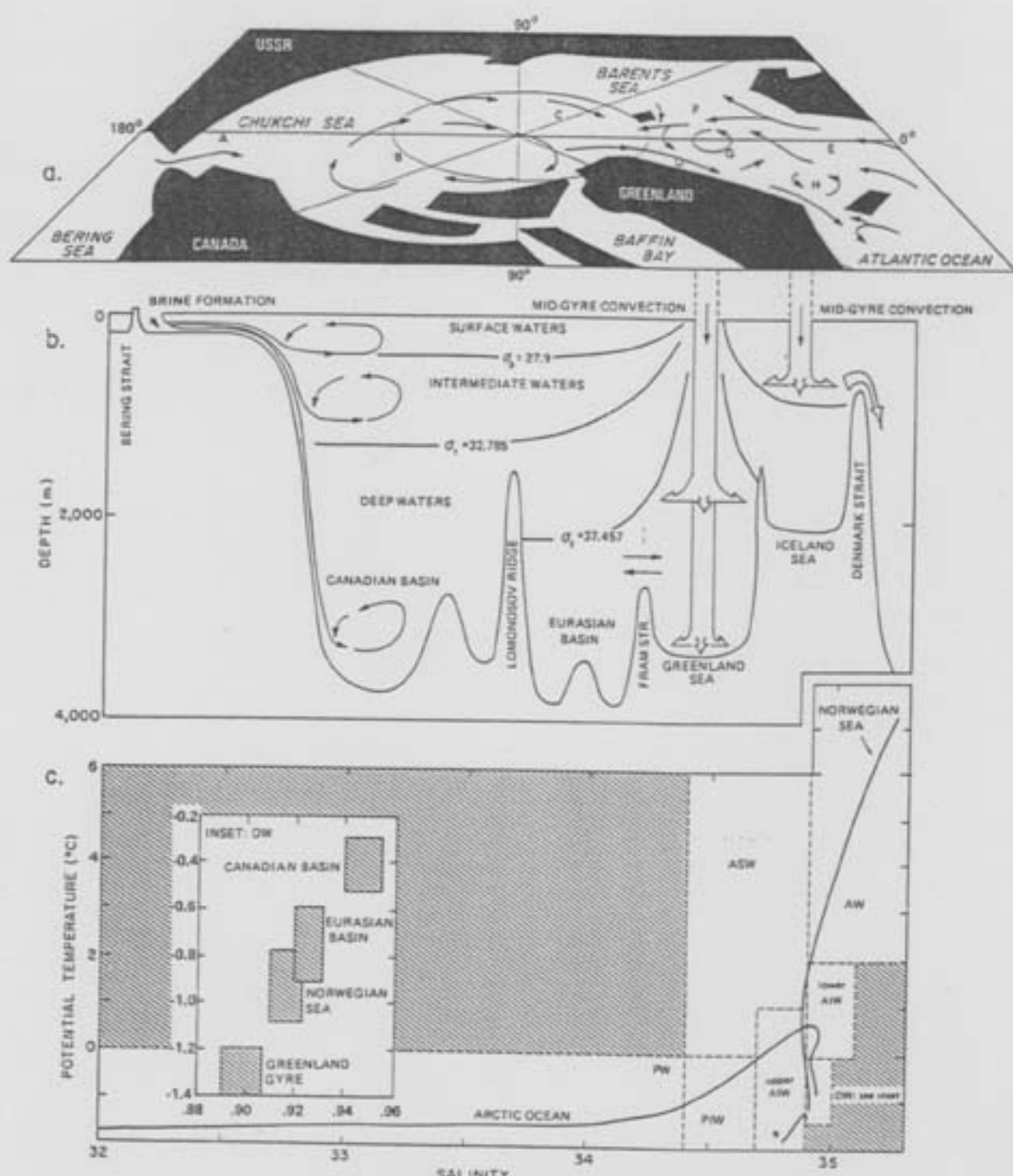


Fig. 11. Schematic circulation and water mass structure in the Arctic Mediterranean. For key to (a) upper ocean circulation, see text. Note that a portion of the relatively warm water carried northward with the West Spitsbergen Current (arrows marked F) continues into the Arctic Ocean, where it sinks and spreads, filling both the Canadian and Eurasian basins at intermediate depths; this is the so-called Atlantic layer. (c) The abbreviated θ/S curve marked with an asterisk is for the Greenland gyre.

significant temperature changes in the GSDW over only a few years [Aagaard, 1968]. We consider it likely, however, that while the balance of the thermohaline processes may shift from time to time, and thereby produce θ/S variations in the various water masses, the basic features of the thermohaline circulation portrayed in Figure 11 have not changed significantly in recent times. We further believe that the patterns of interbasin exchange shown in Figure 11 are well supported by

the data presented in this paper and elsewhere in the literature [e.g., Aagaard, 1981; Swift et al., 1983]. In particular, we note the role of the Lomonosov Ridge in restricting the GSDW from freshening the deep Canadian Basin. This suggests that the Canadian Basin was also in the past more saline than the Eurasian Basin. However, most of the details of the production of deep and intermediate waters required to drive the circulation suggested by Figure 11 are not well established.

Inter basin exchange with ice formation and drift

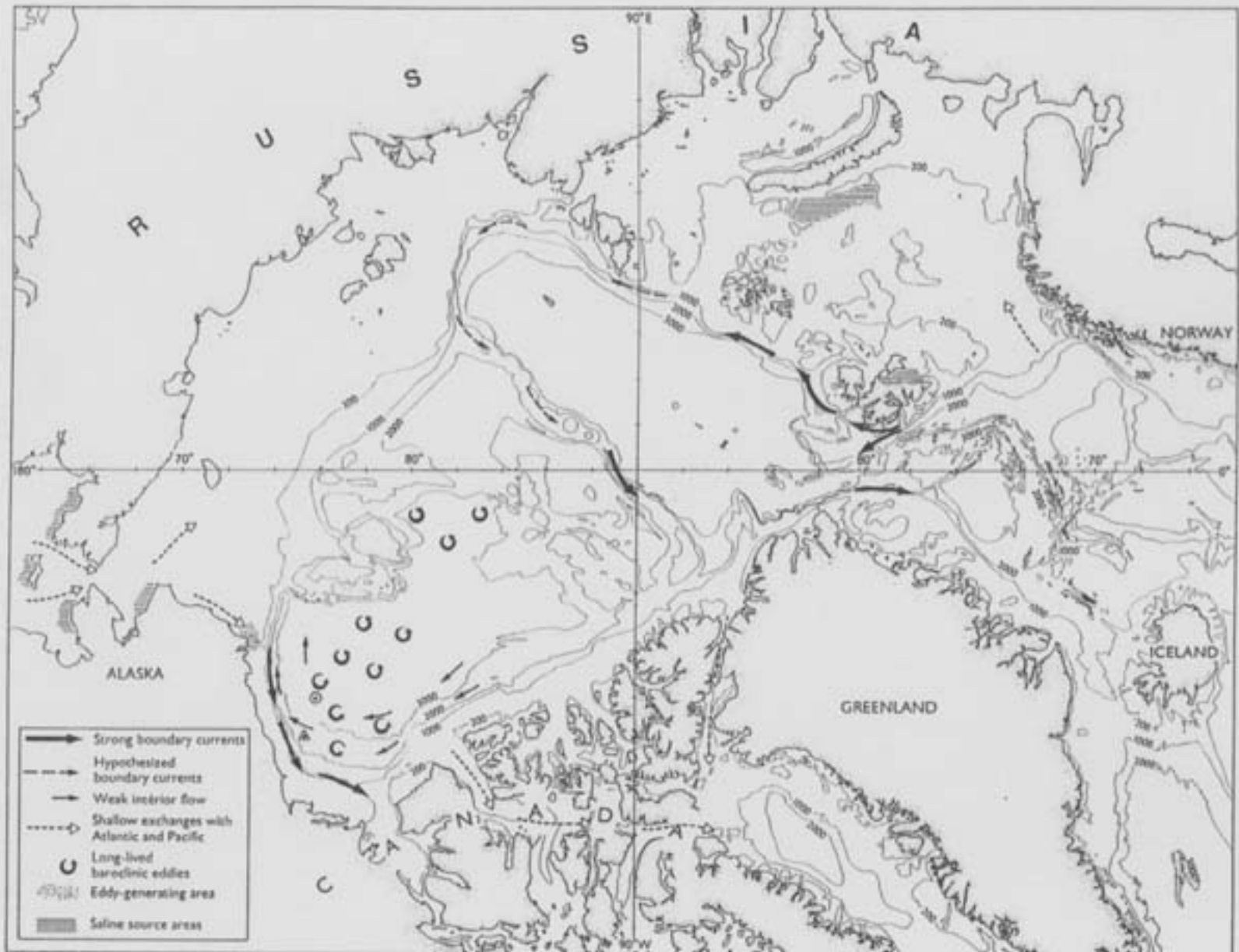


Fig. 4. Schematic subsurface circulation in the Arctic Ocean. Exchanges with the seas to the south generally extend to the sea surface. Known formation areas for saline shelf water and an eddy-generating area are also shown. Location of temperature-salinity measurements shown in Figures 6-9 is indicated by the circle. Location of current measurements shown in Figure 11 is indicated by the triangle. Adapted from Aagaard [1989].

鉛直渦混合

海洋大循環における鉛直混合の役割

深層海洋における熱力学的バランス
→熱塩循環のコントローリングパラメータ

鉛直混合の起源

- 内部重力波の碎波

内部重力波の励起源(とくに深層海洋に対して)
→風, 潮汐, ...

潮汐起源の鉛直混合の空間不均一性(海底地形との相関)
→深層(熱塩)循環の構造

- 二重拡散対流

海洋大循環モデリングにおけるパラメタリゼーションの実情

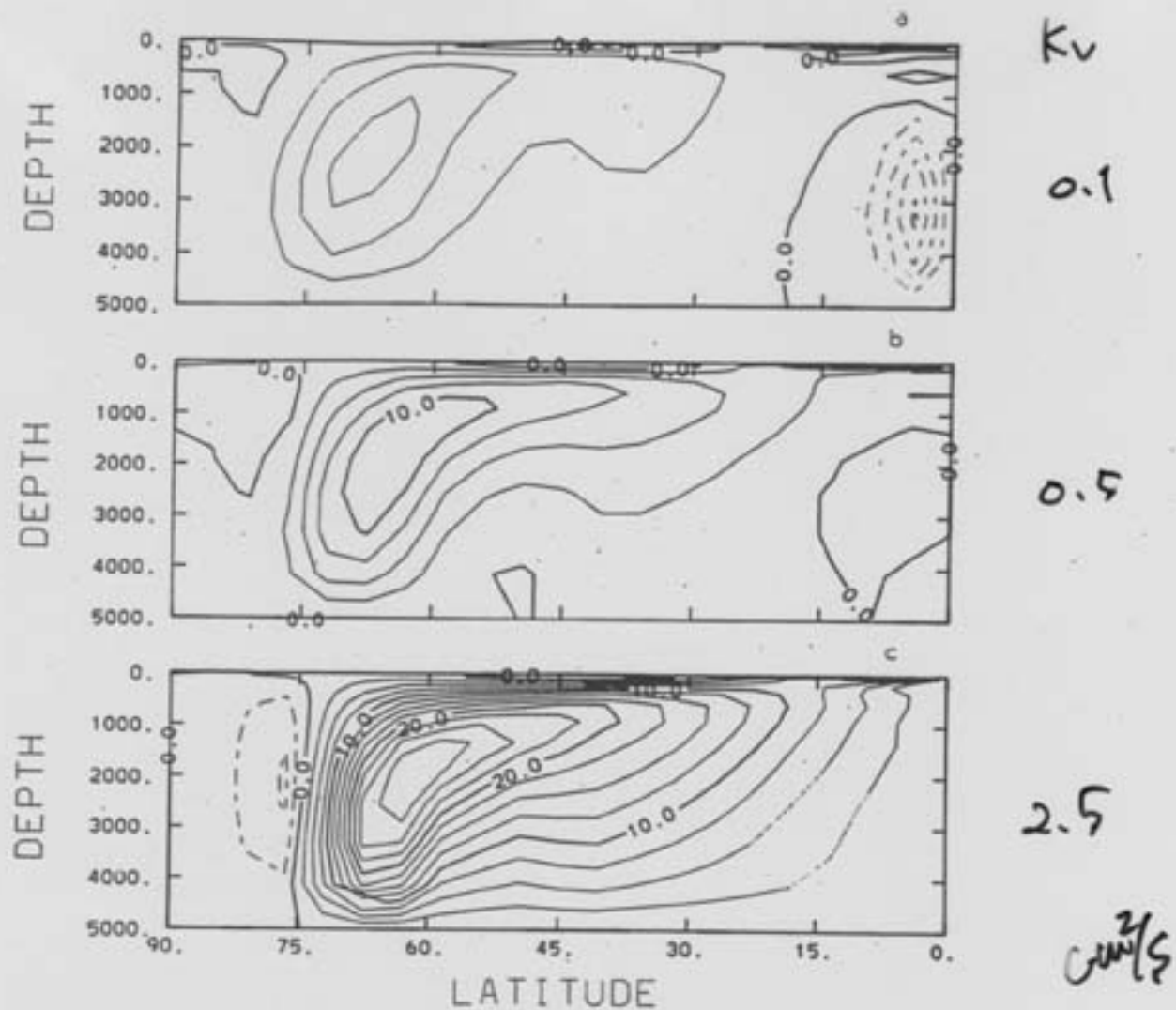


FIG. 7. Meridional overturning streamfunction for (a) $A_{HV} = 0.1$, (b) $A_{HV} = 0.5$, (c) $A_{HV} = 2.5$ (c.i. = $2.5 \times 10^6 \text{ m}^3 \text{ s}^{-1}$, solid contours indicate counterclockwise circulation).

marily due to downwelling on the eastern boundary at the equator. The physical processes driving this circulation are difficult to determine and need further study. Similar features are present in the models of Takano (1981) and Cox and Bryan (1984). Cox and Bryan attribute it to unspecified numerical difficulties. The dependence of the strength of the primary meridional overturning cell on the magnitude of the vertical diffusivity is shown in Fig. 8. The overturning shows an approximately cube root dependence on the diffusivity.

In an analogous manner, we can integrate the continuity equation meridionally, and define a zonal-vertical plane mass transport streamfunction. This quantity is plotted for Experiments 2, 1 and 4 in Fig. 9. The changes in the surface circulation patterns discussed above are very visible here. The increased zonal flow at high diffusivity leads to a much stronger zonal overturning circulation. Further, the upper branch of the circulation extends to greater depth in the high diffusivity case. The dependence of the primary zonal overturning cell on the diffusivity is shown in Fig. 10, in-

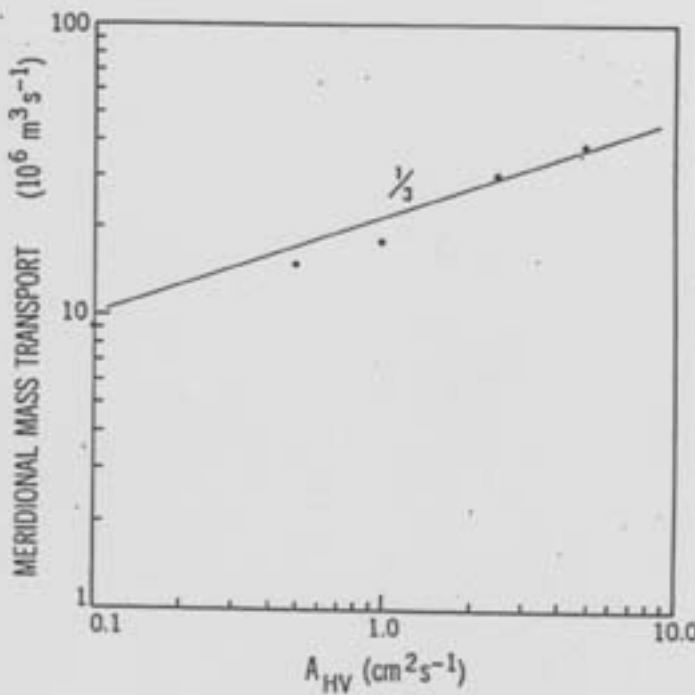
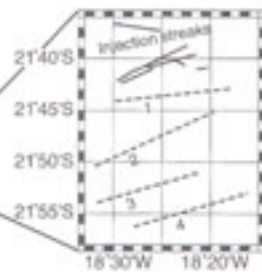
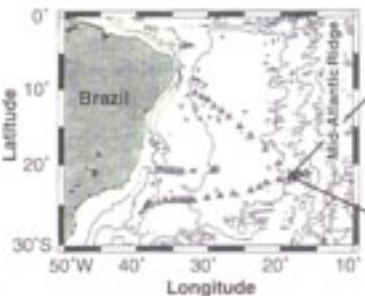
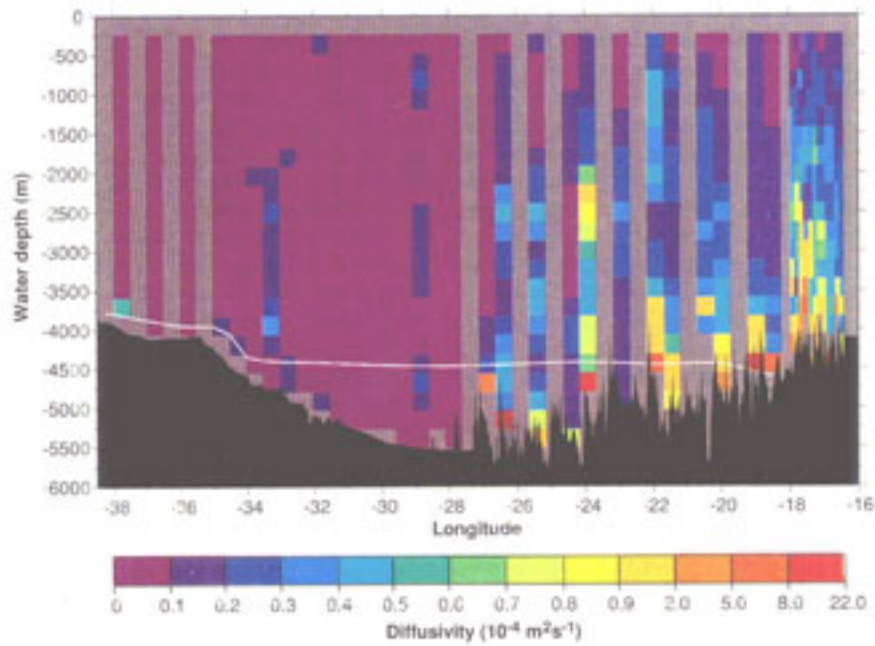


FIG. 8. Dependence of meridional overturning streamfunction on vertical diffusivity.



Brazil Basin



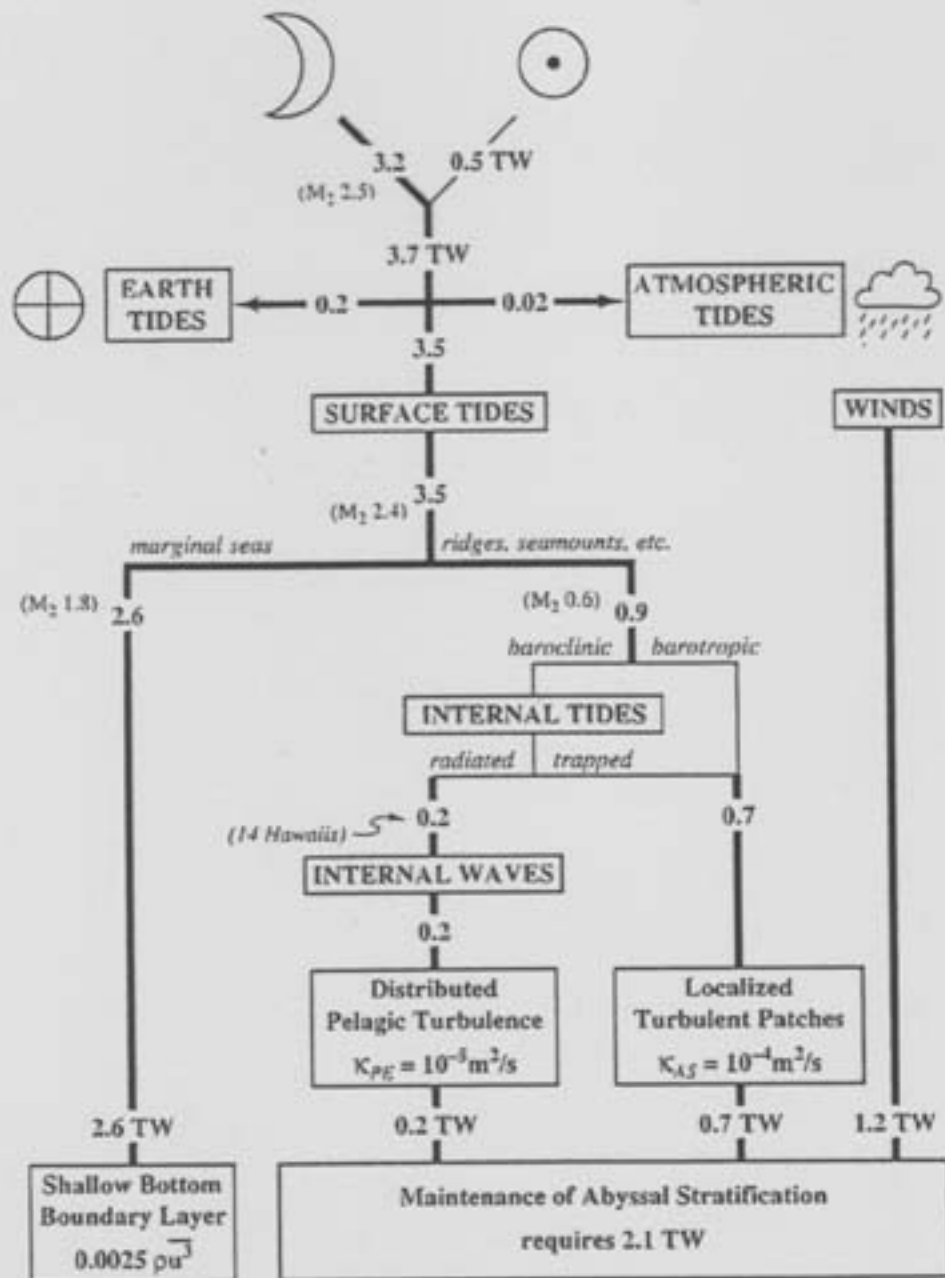


Fig. 4. An impressionistic budget of tidal energy flux. The traditional sink is in the bottom boundary layer (BBL) of marginal seas. Preliminary results from Egbert (1997) based on TOPEX/-POSEIDON altimetry suggest that 0.9 TW (including 0.6 TW of M_2 energy) are scattered at open ocean ridges and seamounts. Light lines represent speculation with no observational support. "14 Hawaiis" refers to an attempted global extrapolation of surface to internal tide scattering measured at Hawaii, resulting in 0.2 TW available for internal wave generation. The wind energy input is estimated from Wunsch (1998), to which we have added 0.2 TW to balance the energy budget. This extra energy is identified as wind-generated internal waves — radiating into the abyss and contributing to mixing processes.

鉛直対流

鉛直対流＝渦運動？

- ここで言う「鉛直対流」の指すもの
- 空間スケールとモデリング

海洋大循環における鉛直対流の役割

深層水形成の起源となる過程

海洋大循環モデルにおけるパラメタリゼーションの方法

対流調節：成層不安定の瞬時の解消

よりよい方法は？

海面境界層(混合層)

海面混合層の実態

海面から深さ数十メートル(ないしそれ以上)に及ぶ一様な層

海洋大循環における海面混合層の役割

中層水の形成過程

混合層を維持するエネルギー源

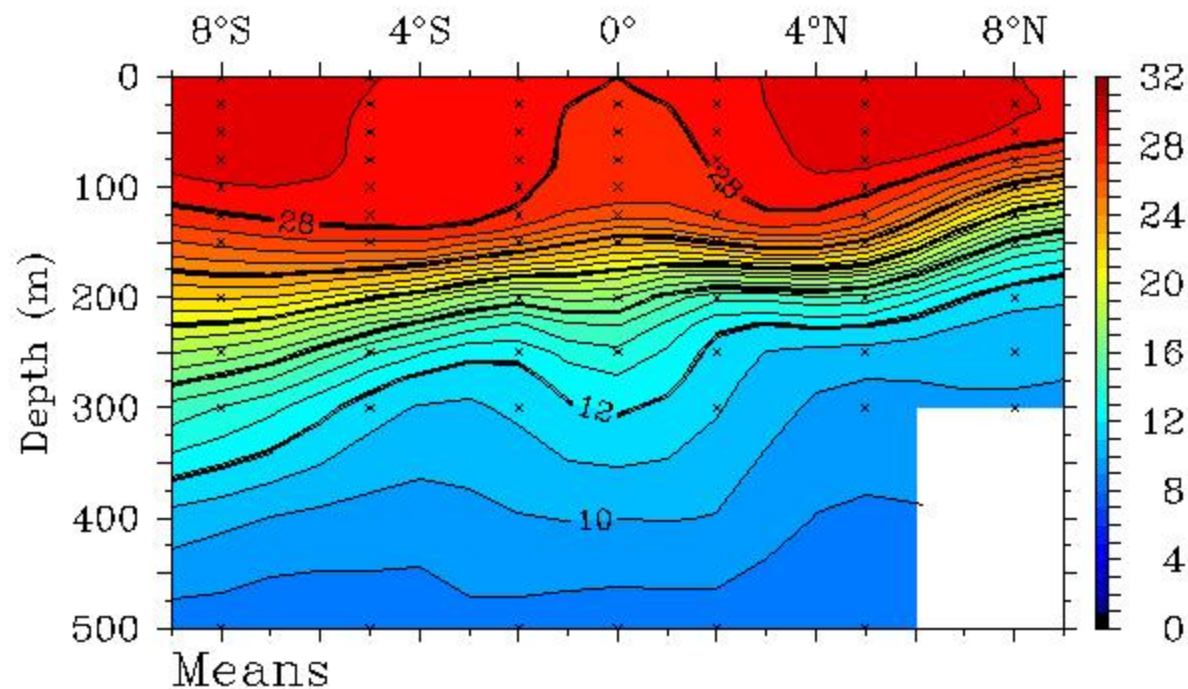
- ・シアによる乱流エネルギー生成
- ・風波の碎波に起因する乱流エネルギー生成
- ・Langmuir 循環

海洋大循環モデルにおけるパラメタライズの方法

- ・バルクモデル
- ・turbulent closure

Monthly Mean TAO/TRITON Temperatures ($^{\circ}\text{C}$)

November 2000 180W



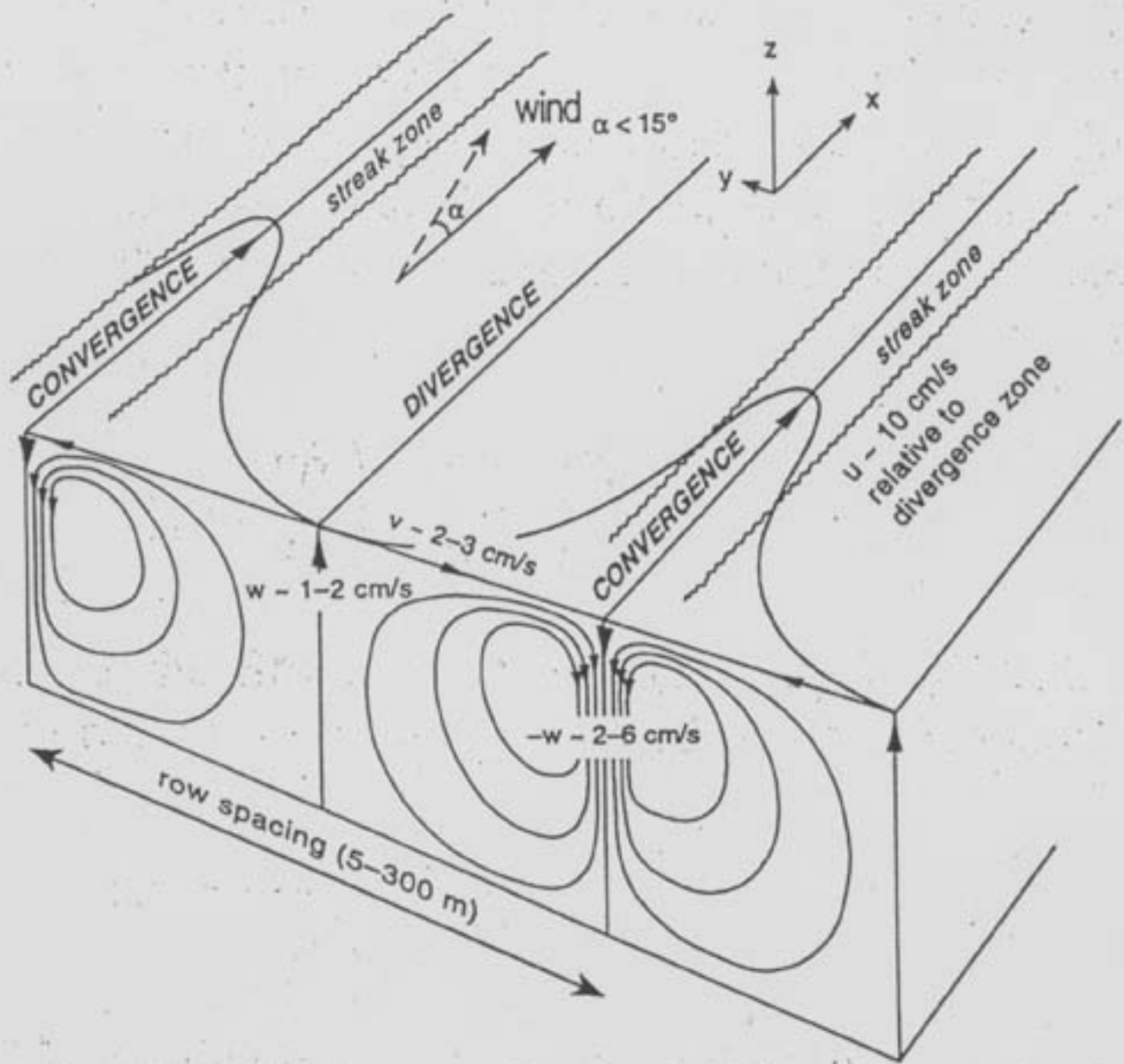


Fig. 1. A schematic representation of Langmuir circulation. (Redrawn from Pollard (1977).)

海底境界層

対象としている現象とその海洋大循環における役割
鉛直対流と深層水塊をつなぐ過程

海底境界層過程の実態

- 海底エクマン層
- 傾圧渦
- エントレインメント

海洋大循環モデルにおけるパラメタリゼーション

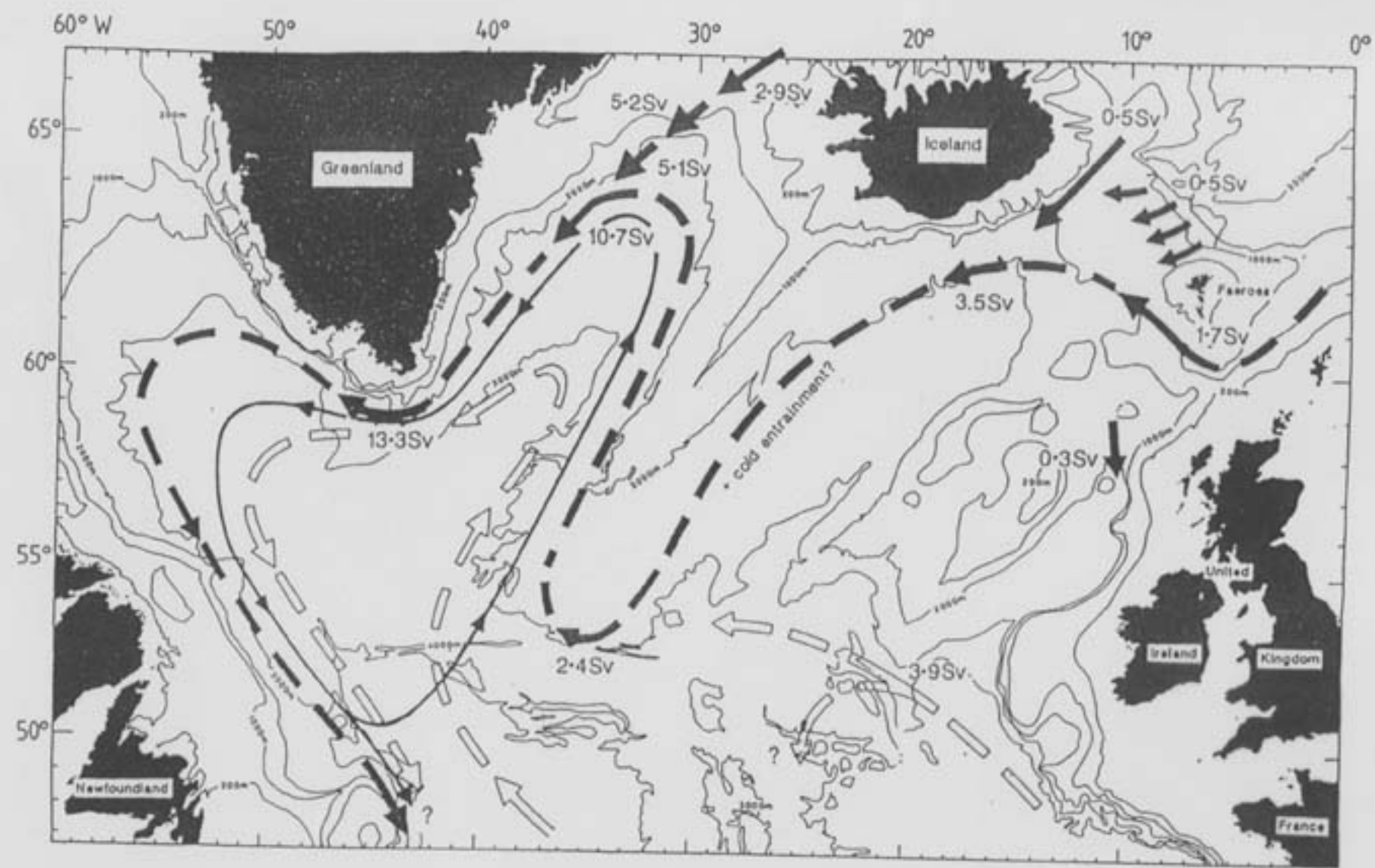


Figure 13. Proposed transport scheme for waters denser than $\sigma\theta = 27.80$ in the northern North Atlantic, based on all available measurements.

Dickson and Brown (1994)

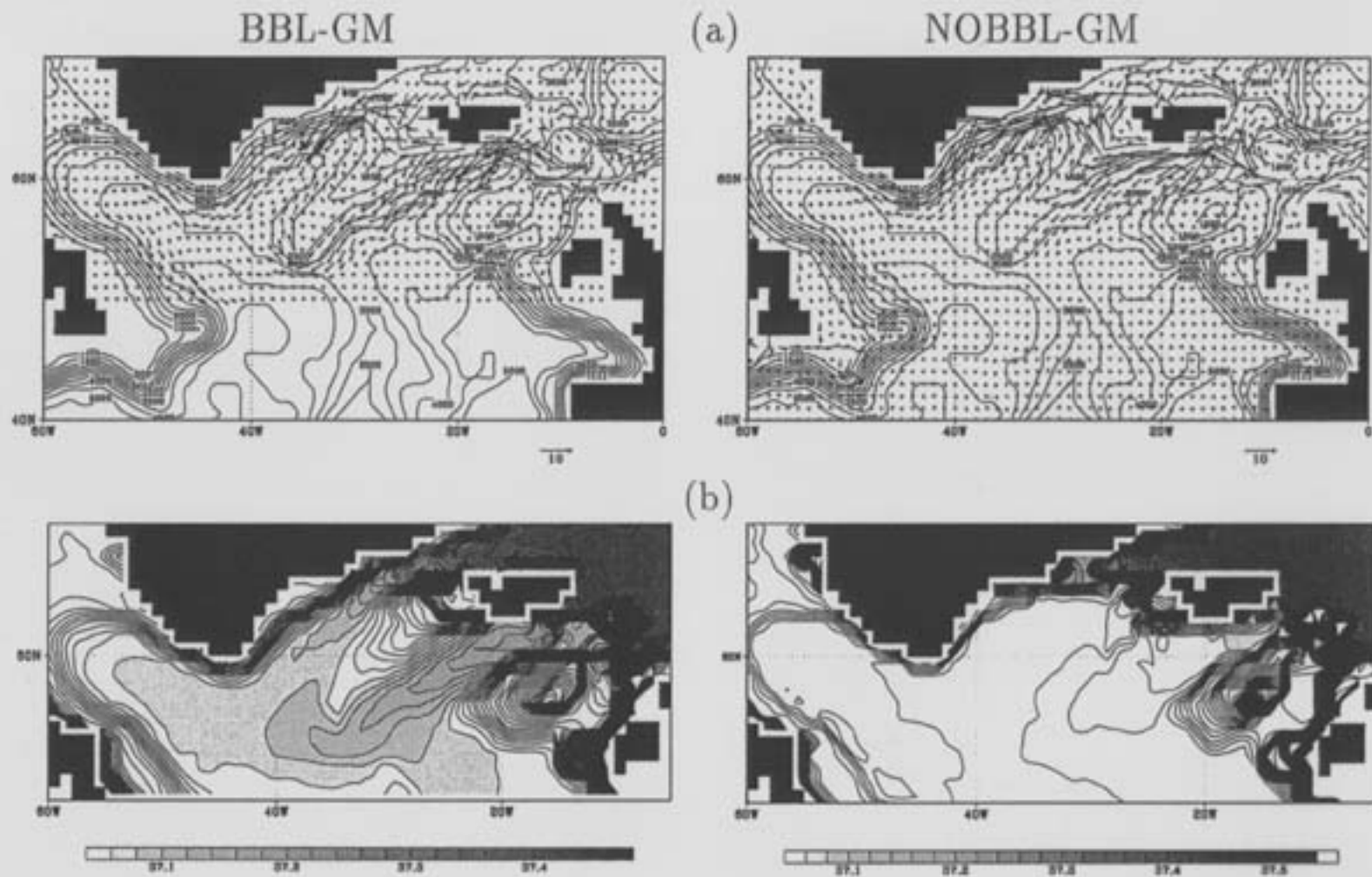


Figure 10: Properties in BBL for BBL-GM (left figures) and near the bottom for NOBBL-GM (right) in the northern North Atlantic: (a) horizontal velocity fields and topography, (b) potential density (σ_2). Counter interval is 500m for (a), 0.02 σ_2 for (b). Shading is imposed more than 37.05 for (b).